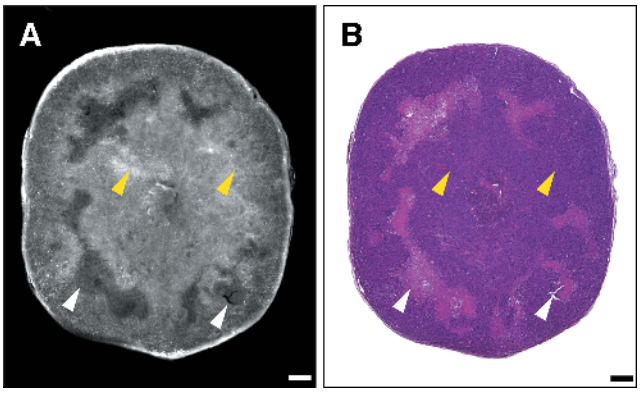

Figure W1. Necrosis evaluation. The morphologic comparison of the virtual tissue slice from the UM (A) and classic H&E staining (B) showed an excellent correlation. Both methods clearly differentiated the necrotic tissue areas (white arrowhead) from the solid tissue areas (yellow arrowhead) of the tumor. Single slices, 5-μm diameter. Scale bar, 250 μm.

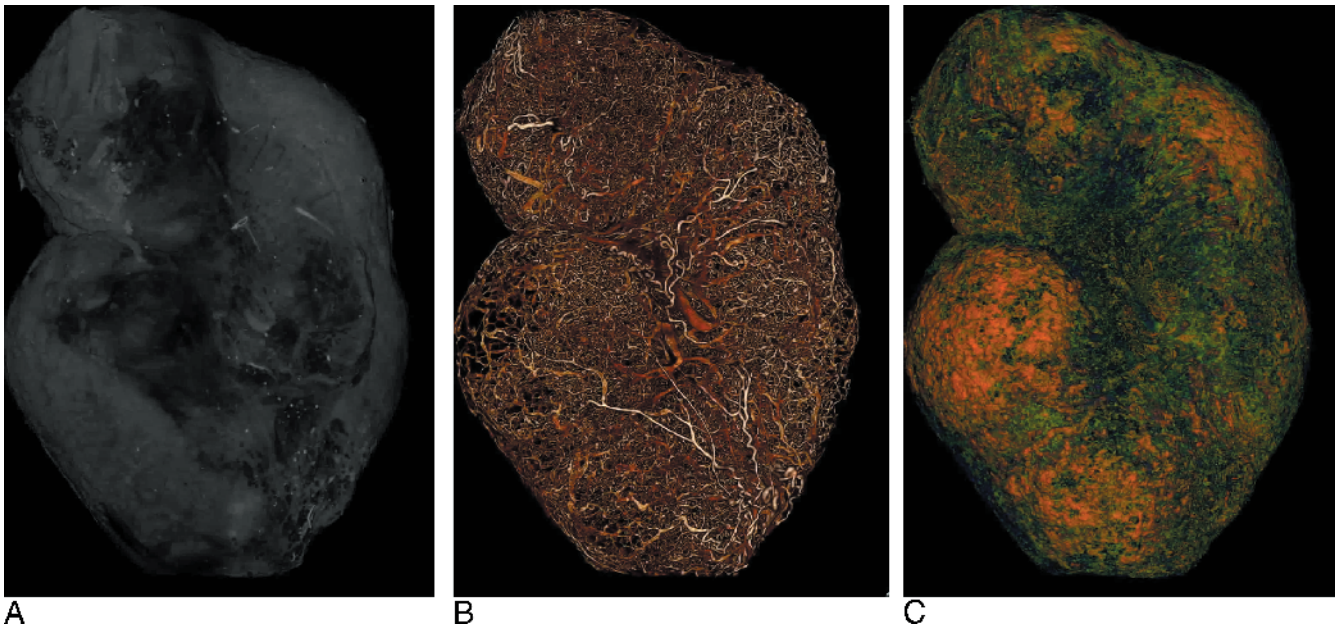

Video W1. Volume rendering of (A) tumor tissue, (B) tumor vessels, and (C) trastuzumab–Alexa 750 penetration in KPL-4 breast tumor.

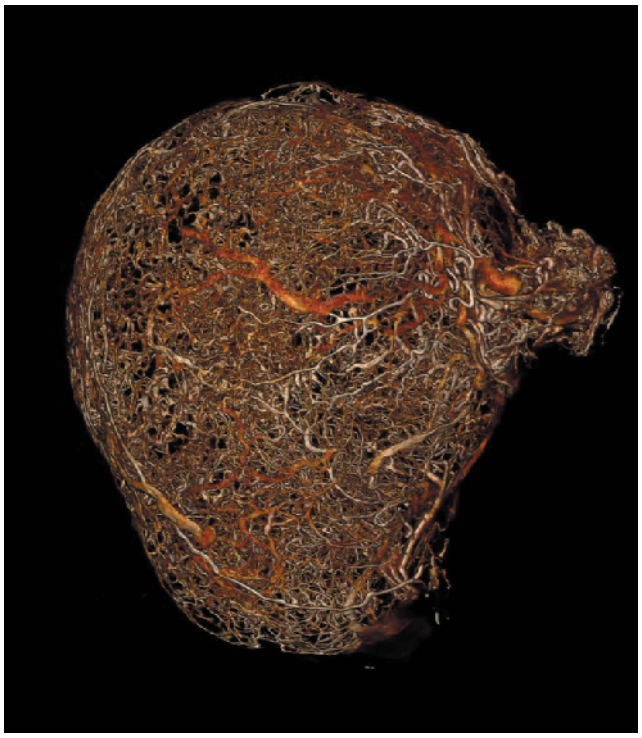

Video W2. Volume rendering of tumor vessel architecture in KPL-4 breast tumor.

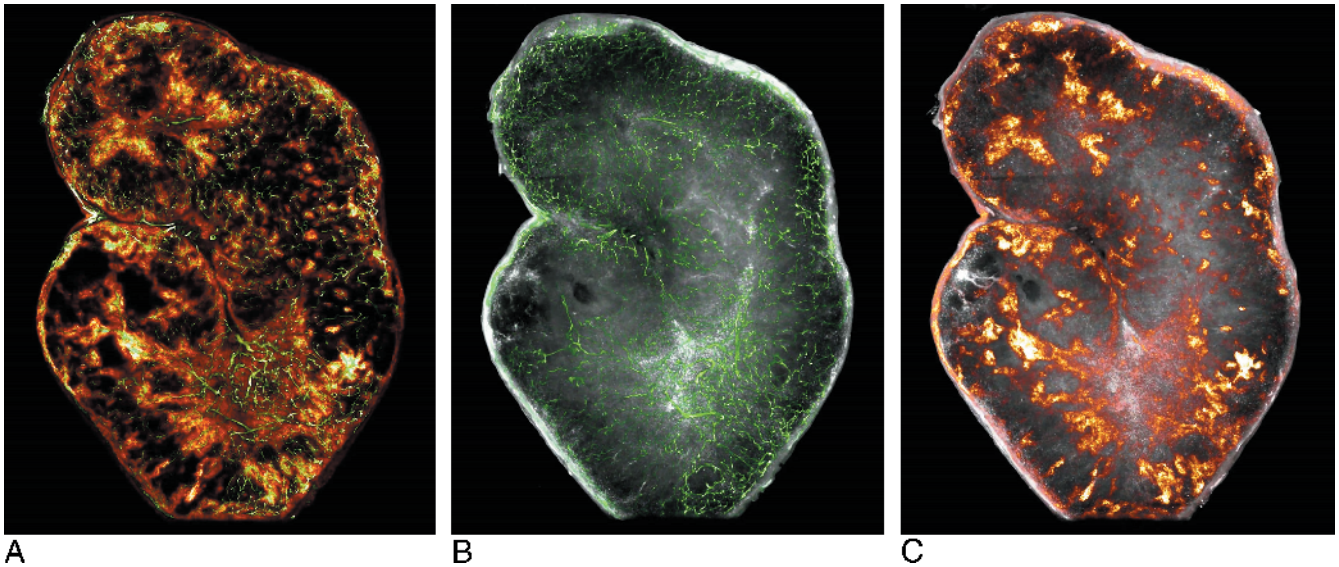

Video W3. MIP (30 slices) overlay of (A) tumor vessels (green) on trastuzumab–Alexa 750 penetration (red), (B) tumor vessels (green) on tumor tissue (gray), and (C) trastuzumab–Alexa 750 penetration (red) on tumor tissue (gray) in KPL-4 breast tumor.

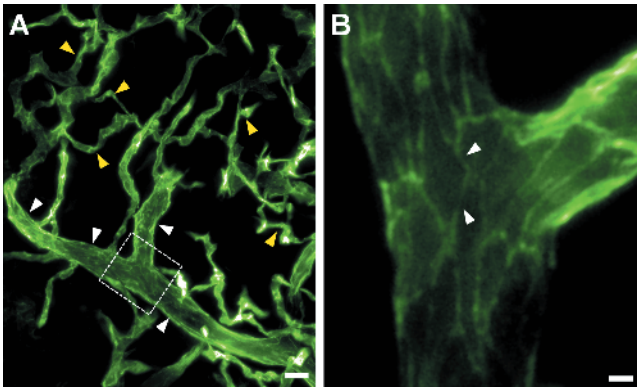

Figure W2. Vessel morphology. (A) If we concentrate only on smaller sections of the tumor, the local xy resolution can be increased to a value of 0.5 μm. This allowed us to visualize the morphologic transition from regular (white arrowhead) to tumor (yellow arrowhead) vascular structures. (B) The digital blowup of the image data from A allowed even single epithelial cells on the surface of the vessels to be visualized (white arrowhead). MIP, (A) 30 slices with 5-μm diameter per slice and (B) 5 slices with 5-μm diameter per slice. Scale bar, (A) 25 μm and (B) 5 μm.

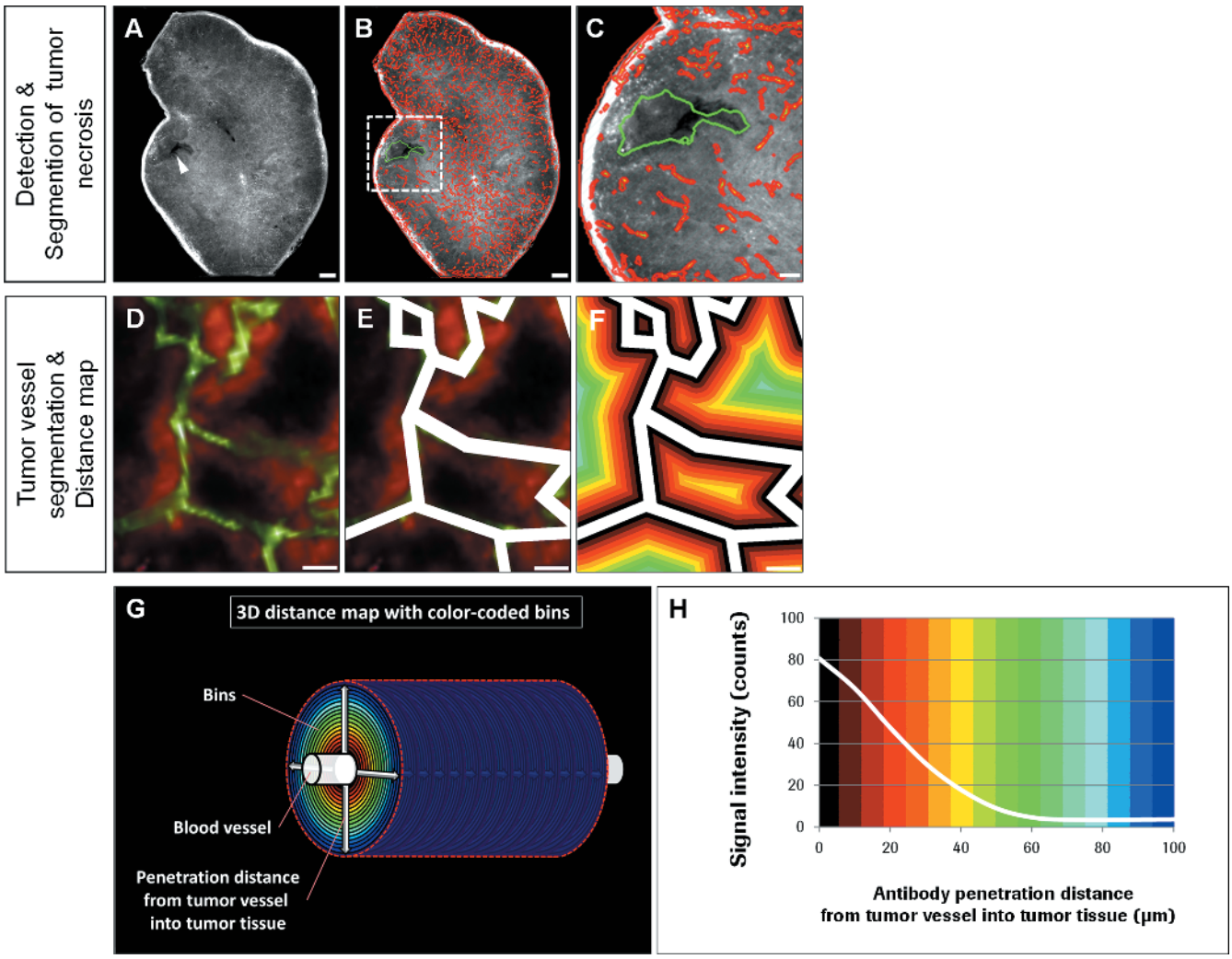

Figure W3. Detection of necrotic tissue areas and quantification of drug penetration. (A) The contrast differences of the tumor tissue allow a rough differentiation between vital and necrotic (white arrowhead) regions. (B) To detect and quantify the necrotic tissue areas, a binary image of the segmented vessels (red) was overlaid on the tissue channel from the UM. We classified tumor areas with no vessels and a minimum distance of 200 μm to the surrounding vasculature as necrotic. We then used a growing strategy to extend those areas up to a minimum vascular distance of 125 μm (green). Scale bar, 250 μm and 100 μm (blowup). (D) We combined the UM information from the tumor vessel (green) and the antibody channel (red) to determine the antibody penetration from the tumor vessels into the surrounding tissue. (E) The vessels were three-dimensionally detected in the whole tumor region. (F and G) After vessel detection, we created a 3D distance map in the tumor region and divided it into individual bins. The different bins are displayed color-coded to allow easy visual differentiation. We then calculated the antibody signal in the various bins. (H) The resulting signal intensity gradient reflects antibody penetration from the tumor vessels into the surrounding tumor tissue. The analysis of antibody penetration from the margin of the tumor to its center follows the same principles. (A–C) MIP, 30 slices with 5-μm diameter per slice. Scale bar, 50 μm.

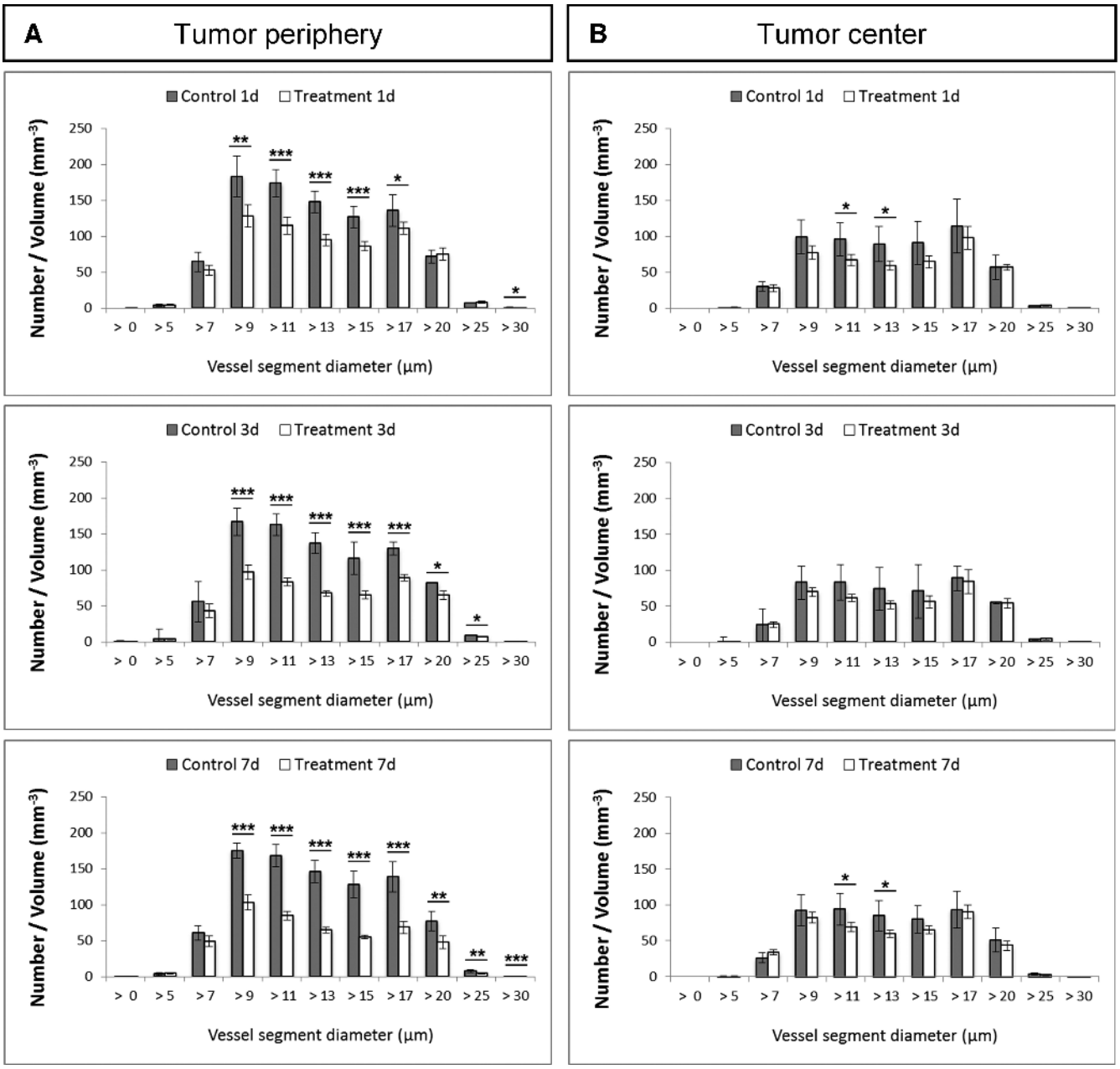

Figure W4. Vessel segment diameter distribution. Diameter distribution of the vascular segments in the tumor periphery (A) and in the tumor center (B) of the control and treatment groups. Treatment with bevacizumab led primarily to a significant reduction in the number of segments located inside the tumor periphery (A), whereas the effect in the tumor center was only marginal (B). Control group, days 1, 3, and 7; $n = 5$ per day. Treatment group, days 1, 3, and 7; $n = 5$ per day. All values are given as means ± SD. *$P < .05$, **$P < .01$, and ***$P < .001$; t test.

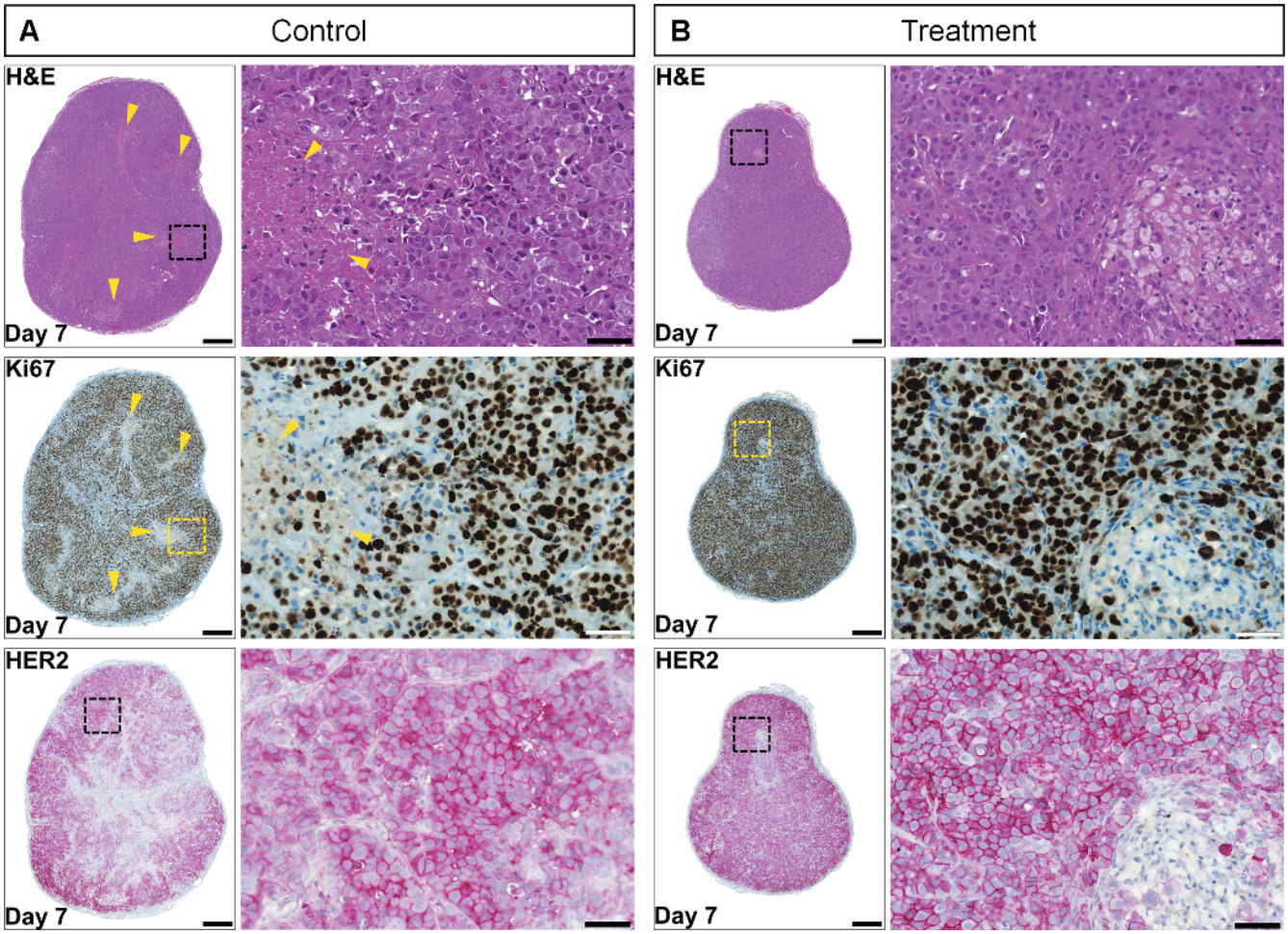

Figure W5. Histologic comparison of the control and treatment groups on day 7. (A) The H&E and Ki67 staining of the control group revealed large areas of necrosis in the tumor tissue (yellow arrowhead). Outside the necrotic tissue areas, the Ki67 staining showed a strong and homogeneous tumor cell proliferation (brown tumor cells). These solid tissue areas also provided a high HER2 expression level on the tumor cell surface. (B) In contrast, the treatment with bevacizumab reduced the necrotic areas in the tumor tissue as shown in the H&E and Ki67 staining. Up to this point, the treatment had no effect on the proliferation rate of the tumor cells. The Ki67 staining showed a strong and homogeneous proliferation pattern similar to the untreated control group. Furthermore, bevacizumab had no direct effect on the HER2 receptor expression level; therefore, the reduced penetration behavior of trastuzumab–Alexa 750 can be only attributed to the antiangiogenic treatment effect. Single slices, 2.5-μm diameter. Scale bar, 500 μm and 50 μm (blowup).

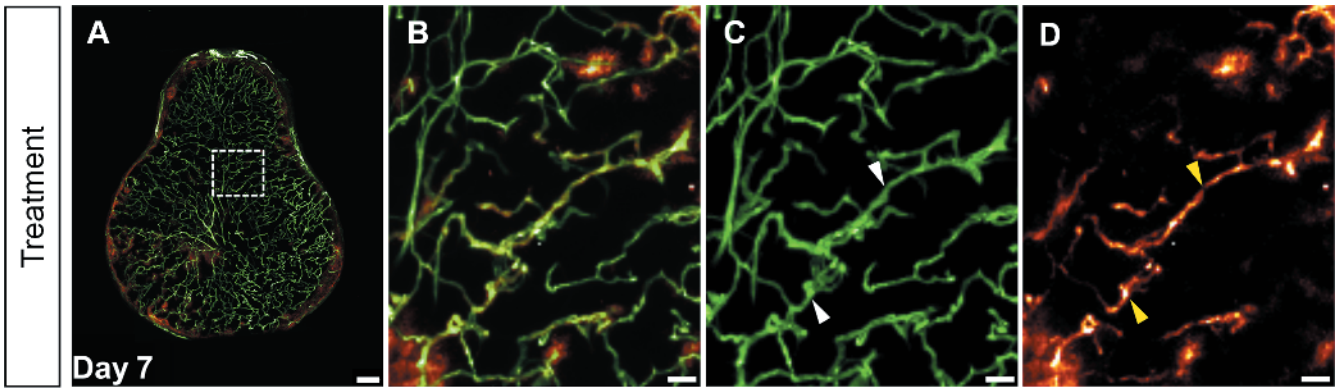

Figure W6. Penetration behavior of trastuzumab–Alexa 750 after bevacizumab pretreatment. (A) The 7-day treatment with bevacizumab led to a reduction, normalization, and homogenization of vascular architecture and significantly reduced trastuzumab–Alexa 750 penetration. (B) The blowup of A clearly shows the reduced penetration of trastuzumab–Alexa 750 from the tumor vessels. In the spectral decomposition of the image from B into the vessel (C) and antibody channel (D), higher levels of residual trastuzumab–Alexa 750 (yellow arrowhead) were detected in the normalized tumor vessels. MIP, 60 slices with 5-μm diameter per slice. Scale bar, 250 μm and 100 μm (blowup).

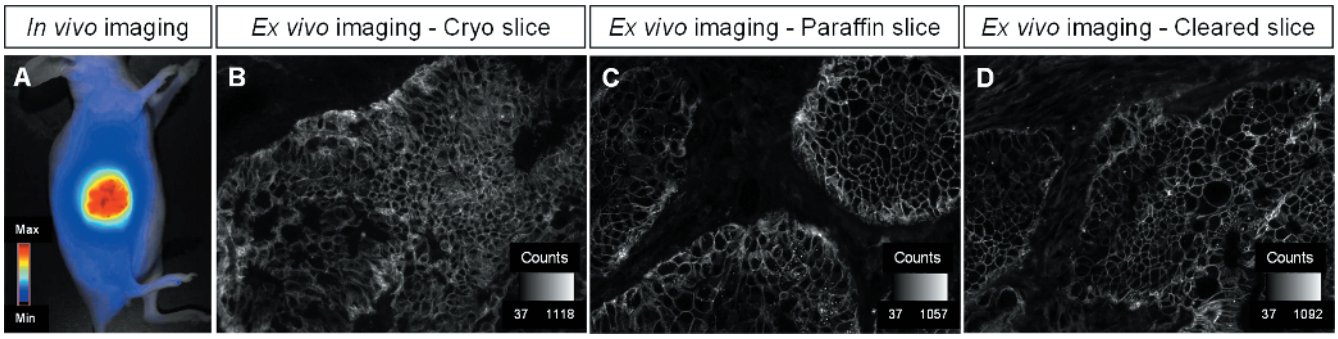

Figure W7. Influence of tumor tissue fixation and optical clearance on the fluorescence signal intensity. (A) HER2-overexpressing non-small cell lung cancer (NSCLC) tumor–bearing mouse was injected i.v. with 2 mg/kg trastuzumab–Alexa 750, and after an incubation time of 24 hours, epifluorescence *in vivo* imaging (Maestro; PerkinElmer, Waltham, MA) was performed. Thereafter, the tumor was explanted and cut into three nearly similar tissue pieces. One tissue section was shortly incubated in liquid nitrogen and stored at a temperature of −80°C. The other two tumor tissue sections were incubated overnight in formalin and dehydrated in a graded ethanol series. Subsequently, one tissue section was incubated in xylene, and the other part was placed for 2 days in a benzylalcohol-benzylbenzoate clearing solution. Afterwards, both tumor sections were embedded in paraffin. Serial tissue slices were prepared from all tumor tissue samples, and the signal intensity of trastuzumab–Alexa 750 was analyzed by fluorescence microscopy (Nuance; PerkinElmer). (B) The fluorescence signal in the cryoslice showed clear and strong binding of trastuzumab–Alexa 750 to the NSCLC cells, and a maximum signal intensity of 1118 counts was detected in the measurement region. (C and D) The maximum fluorescence signal intensity of the labeled antibody in the paraffin (C) and cleared tumor tissue slice (D) was only slightly reduced to 1057 and 1092 counts compared to the cryoslice. The signal reduction can be attributed to the smaller diameter of both tissue slices (2.5 μm *vs* 6 μm for the cryoslice). Identical binding pattern of trastuzumab–Alexa 750 to the tumor cells was clearly visible. No recognizable differences between the cryo-, paraffin, and cleared tumor tissue slices regarding fluorescence signal intensity were detectable. Single slices, (B) 5-μm diameter and (C and D) 2.5-μm diameter.